

Development of polymeric sensing films based on a new tridentate bis(phosphinic amide)-phosphine oxide for determining Europium(III) in water

F. J. Sainz-Gonzalo,^a M. Casimiro,^b C. Popovici,^b A. Rodríguez-Diéguez,^c J. F. Fernández-Sánchez,^{*a} I. Fernández,^{*b} F. L. Ortiz,^{*b} A. Fernández-Gutiérrez^a

^a Department of Analytical Chemistry, Faculty of Sciences, University of Granada, Av. Fuentenueva s/n, 18071 Granada, Spain. Fax: +34 958243328; E-mail: ifferman@ugr.es

^b Laboratory of Organic Chemistry, University of Almería, Ctra. Sacramento s/n, 04120 Almería, Spain. Fax: +34 950 015481; Tel: +34 950 015648; E-mail: ifferman@ual.es

^c Department of Inorganic Chemistry, Faculty of Sciences, University of Granada, Av. Fuentenueva s/n, 18071 Granada, Spain. Fax: +34-958248526.

Contents:

- Chemical and Reagents
- Figure S1. ESI-TOF mass spectra in the positive ion mode calculated and simulated of **2** and **4**.
- Figure S2. IR (KBr disk) spectra of **2** and **4**.
- Figure S3. ³¹P NMR (202.4 MHz) spectrum of **2** in CD₃CN at RT.
- Figure S4. ¹³C and DEPT-135 NMR (75.5 MHz) spectrum of **2** in CD₃CN at RT.
- Table S1. ¹H isotropic shifts (δ_{iso}) for complex **2** at 300 MHz in CD₃CN at 25 °C.
- Table S2. ¹H isotropic shifts (δ_{iso}) for complex **4** at 300 MHz in CD₃CN at 25 °C.
- Figure S5. ¹H EXSY NMR spectrum ($t_m = 500$ ms) of **2** in CD₃CN at RT.
- Figure S6. ¹H, ¹³C gHMQC NMR spectrum of **2** in CD₃CN at RT.
- Figure S7. ¹H, ¹³C gHMBC NMR spectrum of **2** in CD₃CN at RT.
- Figure S8. ¹H, ¹³C gHMQC and gHMBC NMR expansions of the NiPr₂ region for complex **2**.
- Figure S9. X-Ray structures overlay of [Eu(**1**)Cl₃] (**4**) and [Y(**1**)(NO₃)₃] (**5**).
- Figure S10. Response of the complex luminescence intensity versus Ligand:Eu³⁺ ratio and Eu³⁺:Ligand ratio.
- Figure S11. TGA spectrum for complex **2** at the heating rate of 10°C/min under N₂ atmosphere.
- Figure S12. Luminescence intensity versus EtOH percentage in solution.
- Figure S13. Influence of NaCl concentration on the luminescence intensity in solution.
- Figure S14. The pH effect on the complex luminescence intensity in solution.
- Figure S15. The plasticizer effect on the luminescence signals of the membrane sensors.
- Figure S16. Luminescence intensities of the membrane sensors versus DOS plasticizer percentage.
- Figure S17. The joint effect of the ligand and ionic additive percentages on the luminescence responses of the membrane sensors.
- Figure S18. The pH effect on the luminescence signals of the europium sensors.
- Figure S19. Effect of the ionic strength on the luminescence signals of the membrane sensors.
- Figure S20. Calibration graph of europium(III) membrane sensors.
- Figure S21. Variation of the luminescence emission in solution versus time.

Chemical and reagents

Hydrate chloride salts of the lanthanides used were all of the highest purity available and were obtained from ABCR. Bis(2-ethylhexyl) adipate (DOA), 2-nitrophenyloctyl ether (NPOE), potassium tetrakis(4-chlorophenyl) borate (KTPClPB), high molecular weight poly vinyl chloride (PVC) and succinic acid were purchased from Fluka. Bis(2-ethylhexyl) sebacate (DOS) and dioctyl phthalate (DOP) were obtained from Aldrich. Absolute ethanol, anhydrous sodium acetate and potassium hydrogen phthalate were purchased from Panreac. Tetrahydrofurane (THF) was obtained from Lab-Scan. Deuterated chloroform and acetonitrile were purchased from Cambridge Isotope Laboratories, Inc. Sodium chloride was purchased from Riedel-de Haën. Neutral dihydrate sodium citrate was obtained from Merck. D-tryptophan was purchased from Sigma. All chemicals and reagents were of analytical grade except for bis(2-ethylhexyl) sebacate (reagent grade) and were used as received without further purification.

Aqueous solutions were prepared using doubly distilled water obtained from a Milli-Q Plus 185 ultrapure water system (Millipore, Billerica, USA). Stock and working standard solutions of ligand 1 and lanthanide ions were stored in amber glass bottles at 4 °C.

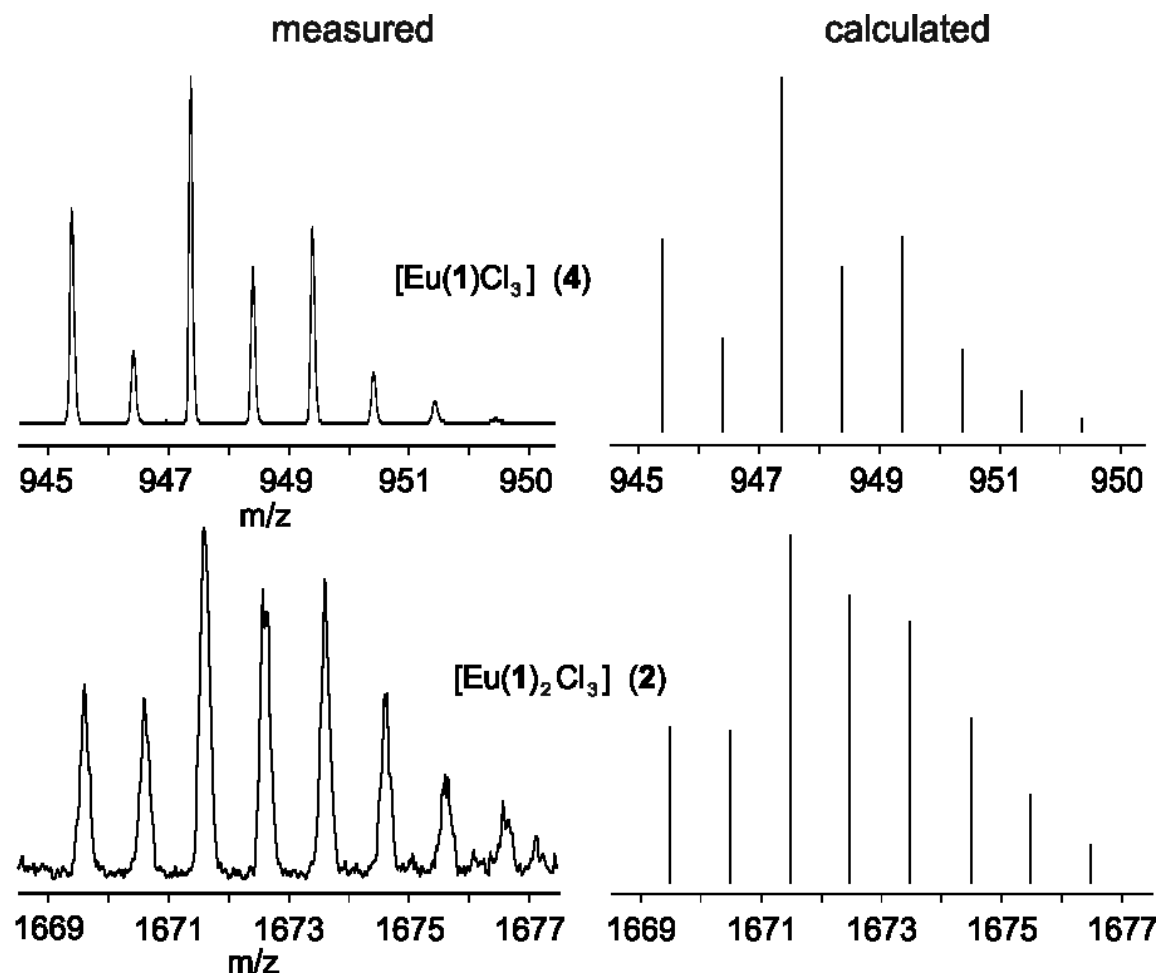


Figure S1. ESI-TOF mass spectra in the positive ion mode calculated and simulated of **2** and **4** in CD_3CN . Note that the optical range for TOF analyzers is below *ca.* 1500 and therefore a significant reduction in the signal/noise is observed.

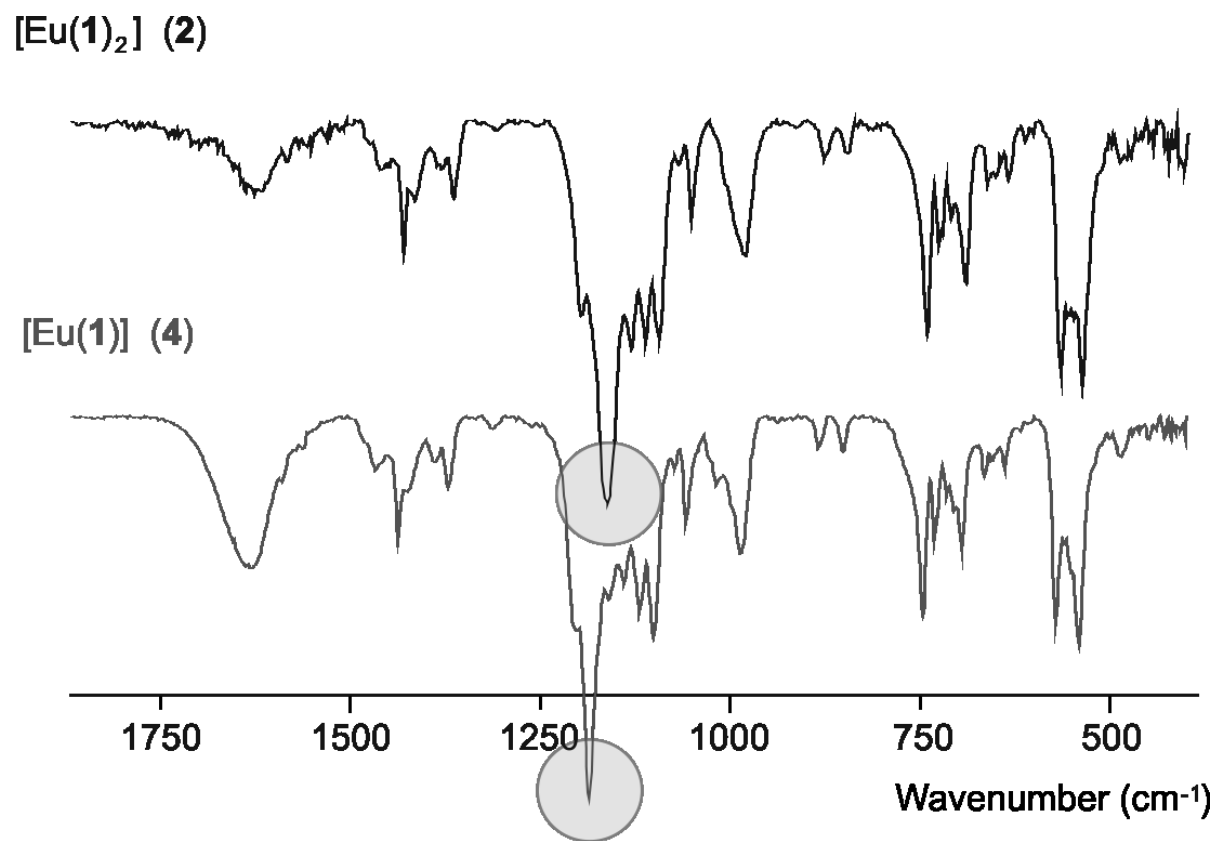


Figure S2. IR (KBr disk) spectra of **2** and **4**.

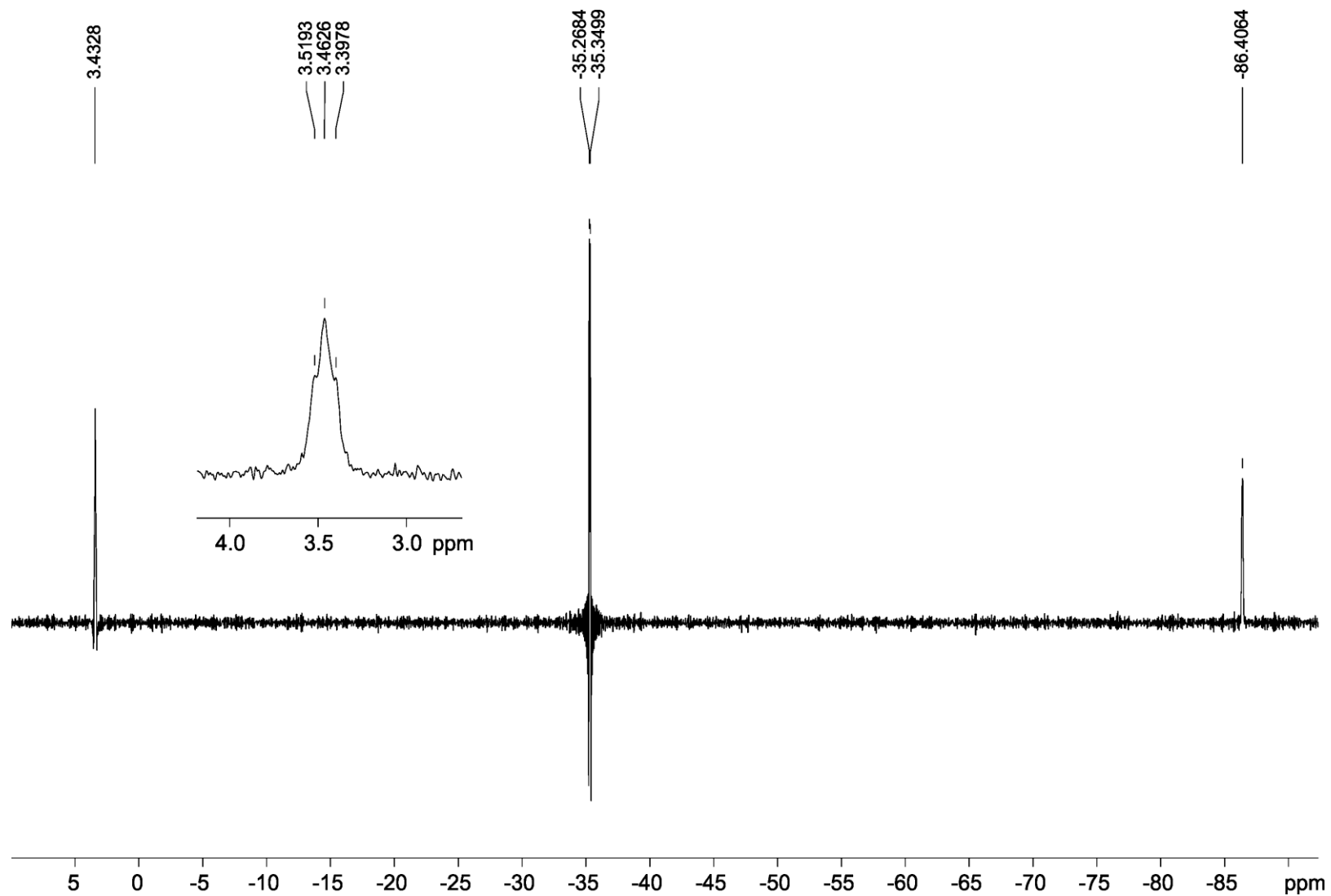


Figure S3. ^{31}P NMR (202.4 MHz) spectrum of **6** in CD_3CN at RT.

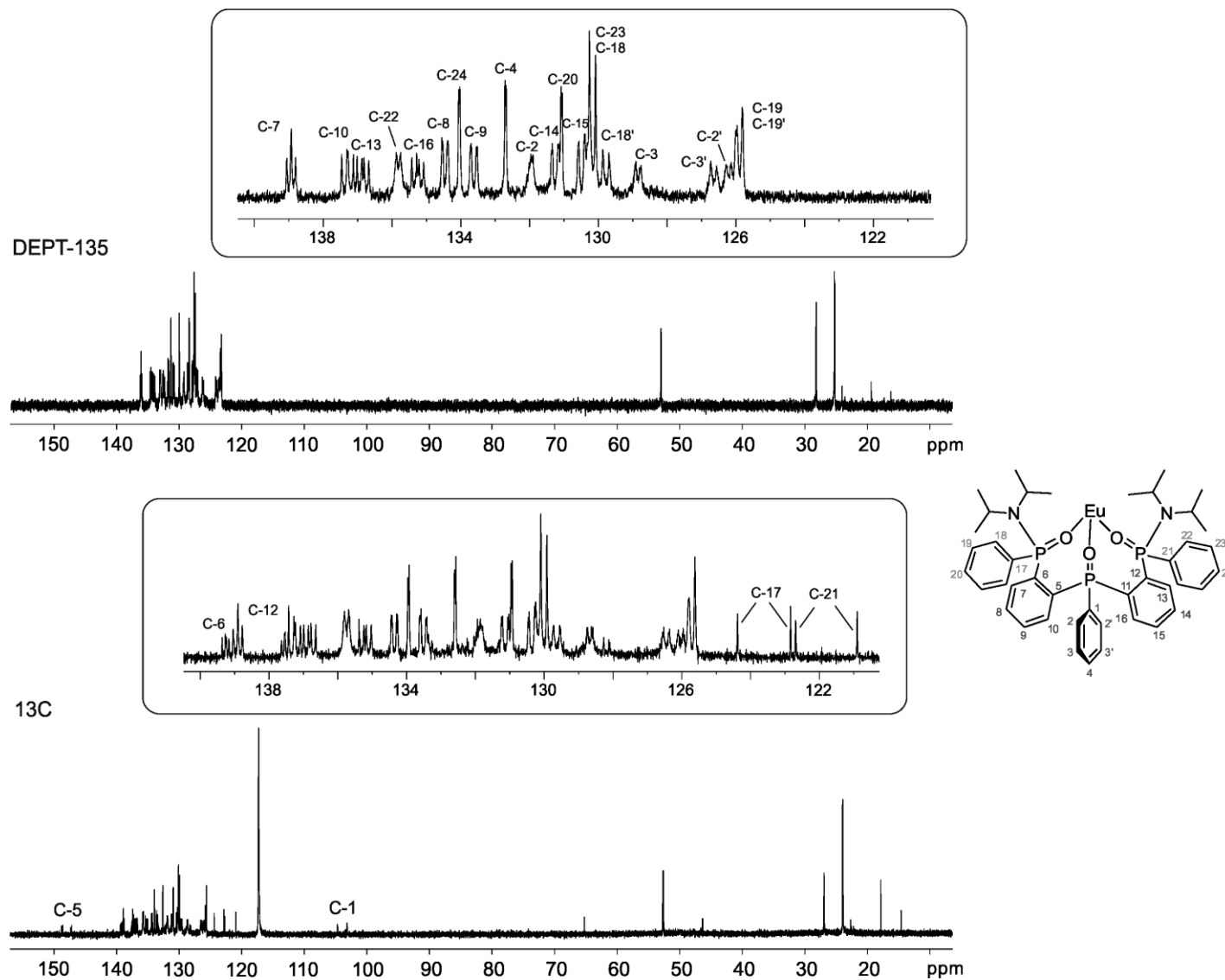


Figure S4. ^{13}C and DEPT-135 NMR (75.5 MHz) spectrum of **2** in CD_3CN at RT.

Table S1. ¹H isotropic shifts (δ_{iso}) for complex **2** at 300 MHz in CD₃CN at 25 °C.

		[Eu(1) ₂ Cl ₃] (2)	[Y(1) ₂ (NO ₃) ₃] (3)	δ_{iso}
Ring I	H-2	4.42	8.58	4.16
	H-2'	4.58	6.56	2.01
	H-3	6.28	7.90	1.62
	H-3'	6.79	7.48	0.69
	H-4	7.16	7.85	0.69
Ring II	H-7	9.88	8.38	-1.50
	H-8	8.66	7.98	-0.68
	H-9	7.93	7.65	-0.28
	H-10	6.14	7.00	0.86
Ring III	H-18	-0.88	8.07	8.95
	H-18'	5.96	7.13	1.17
	H-19	4.85	6.90	2.05
	H-19'	5.96	7.13	1.17
	H-20	5.96	7.13	1.17
Ring II'	H-13	6.23	6.48	0.25
	H-14	5.89	6.88	0.99
	H-15	5.45	6.98	1.53
	H-16	3.93	7.02	3.09
Ring III'	H-22	8.77	8.20	-0.57
	H-22'	8.77	8.20	-0.57
	H-23	8.22	7.79	-0.43
	H-23'	8.22	7.79	-0.43
	H-24	8.50	7.79	-0.71

Table S2. ¹H isotropic shifts (δ_{iso}) for complex **4** at 300 MHz in CD₃CN at 25 °C.

		[Eu(1) ₂ Cl ₃] (4)	[Y(1) ₂ (NO ₃) ₃] (5)	δ_{iso}
Ring I	H-2	4.84	7.53	2.69
	H-2'			
Ring II	H-3	6.70	7.10	0.4
	H-3'			
	H-4			
	H-7	12.34	8.56	3.78
Ring III	H-8	9.24	8.04	1.2
	H-9	8.09	7.37	0.72
	H-10	6.78	6.47	0.31
	H-18	5.67	7.80	2.13
Ring II'	H-18'			
	H-19	5.17	7.23	2.06
	H-19'			
	H-20		7.80	
Ring III'	H-13	6.03	6.34	0.31
	H-14	7.06	6.34	0.72
	H-15	7.41	6.70	0.71
	H-16	7.94	7.07	0.87
Ring III'	H-22	8.95	8.32	0.63
	H-22'			
	H-23	8.02	7.80	0.22
	H-23'			
	H-24	3.43		

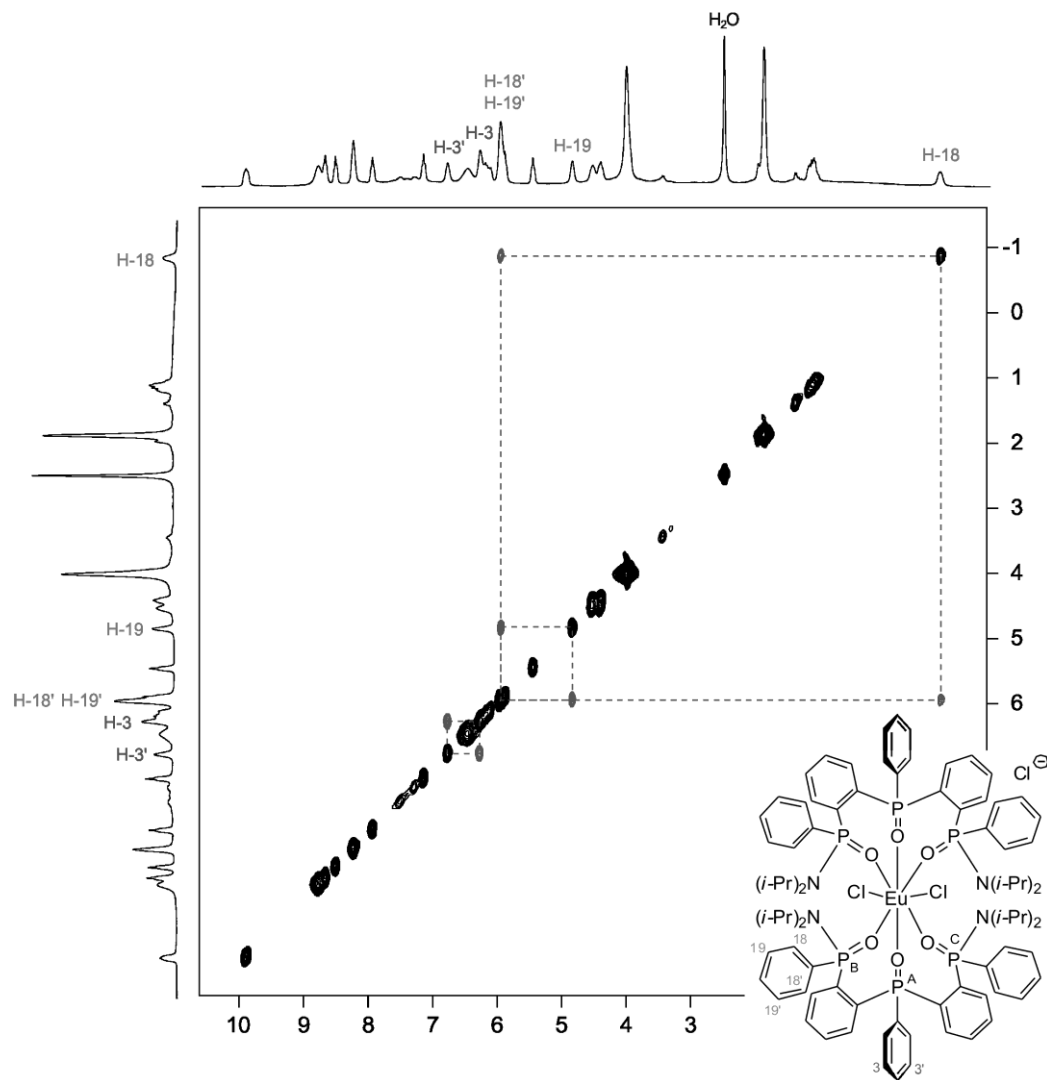


Figure S5. ^1H EXSY NMR spectrum ($t_m = 500$ ms) of **2** in CD_3CN at RT.

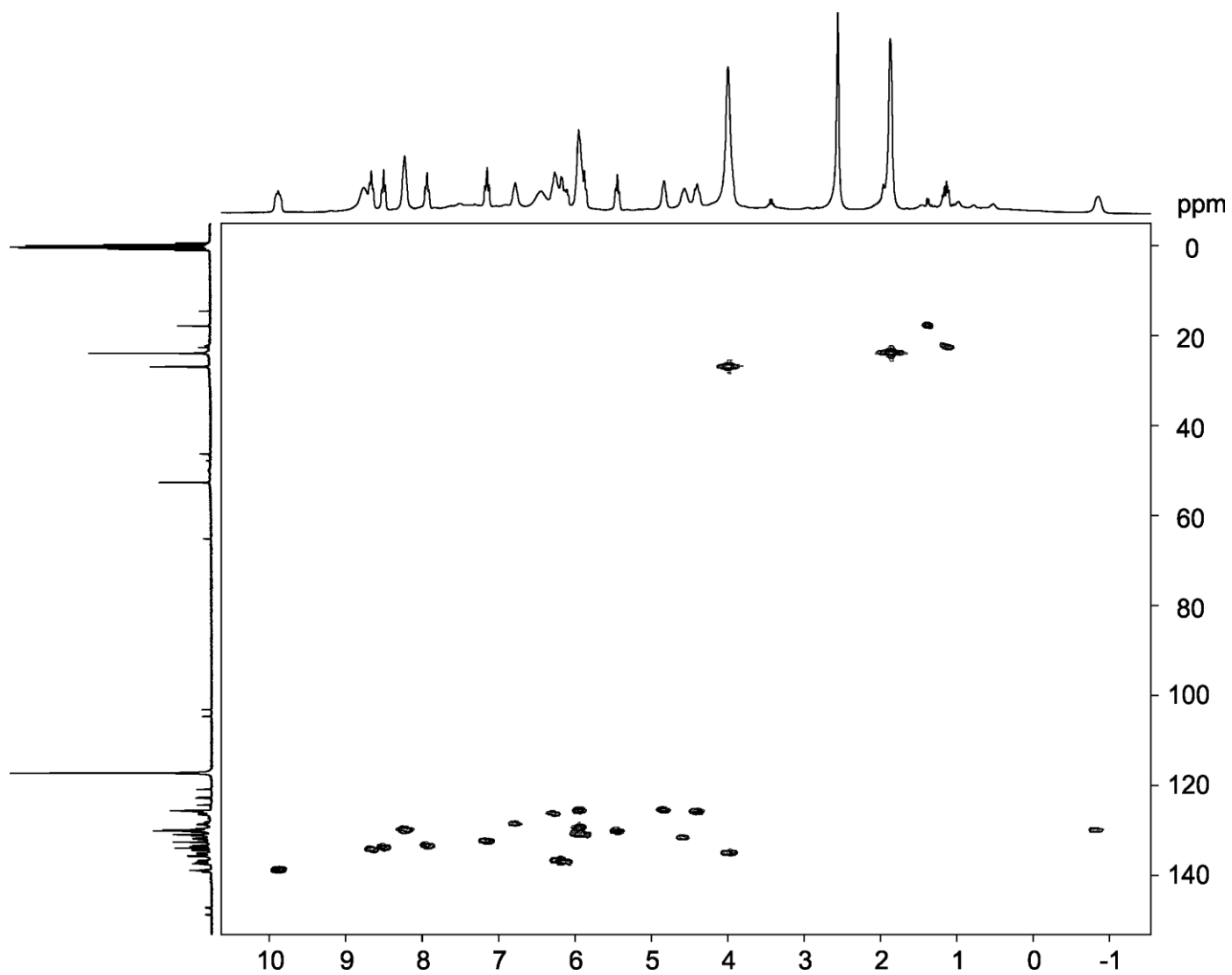


Figure S6. ^1H , ^{13}C gHMQC NMR spectrum of **2** in CD_3CN at RT.

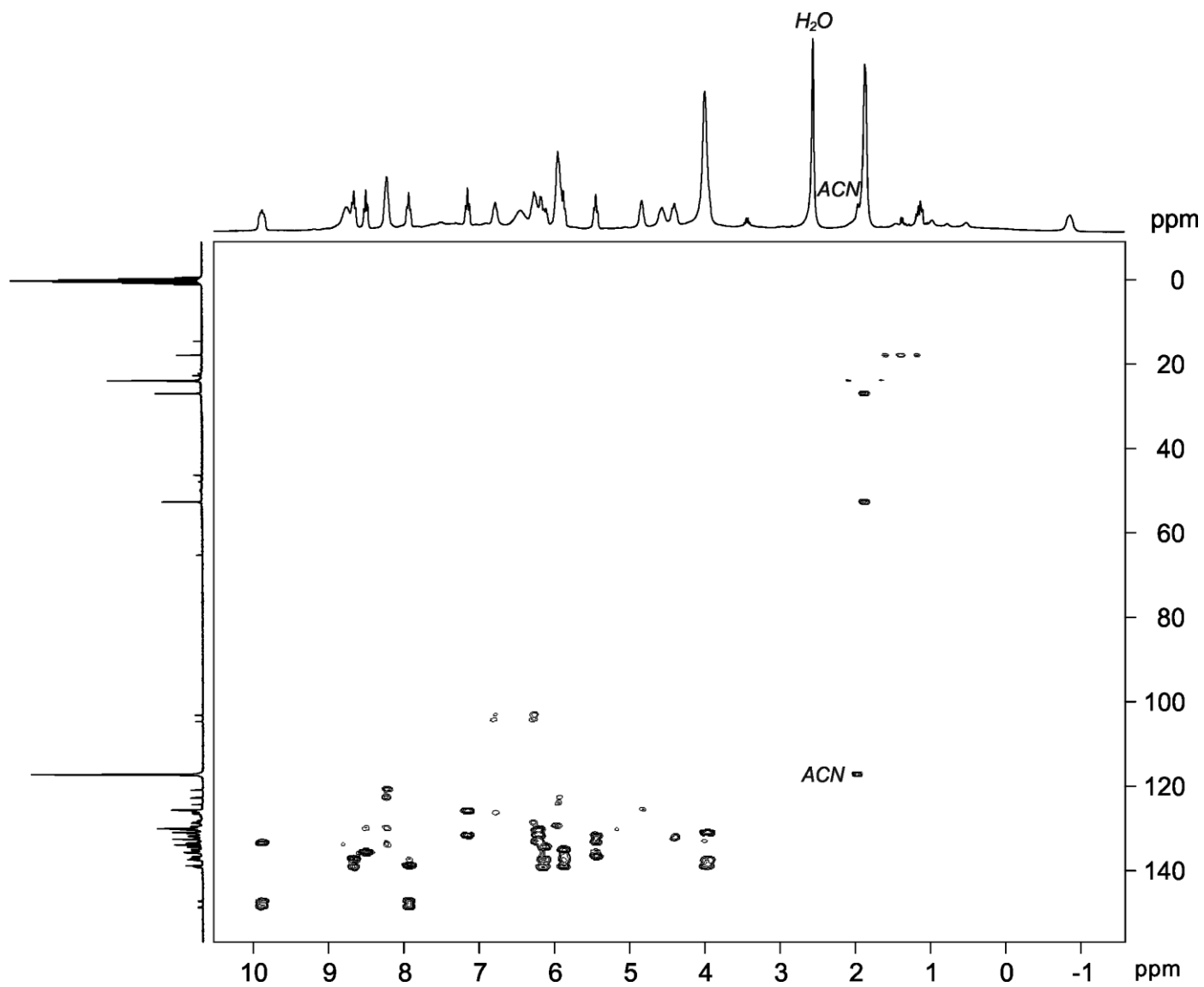


Figure S7. ^1H , ^{13}C gHMBC NMR spectrum of **2** in CD_3CN at RT.

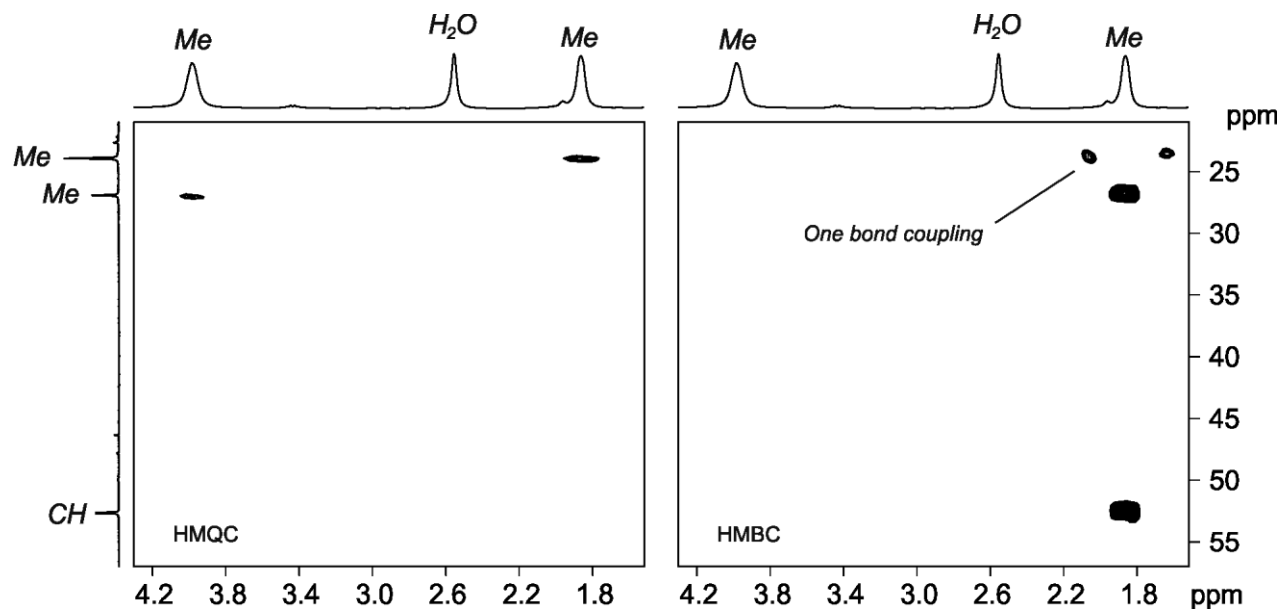


Figure S8. ¹H, ¹³C gHMQC and gHMBC NMR expansions of the NiPr₂ region for complex **2** in CD₃CN at RT.

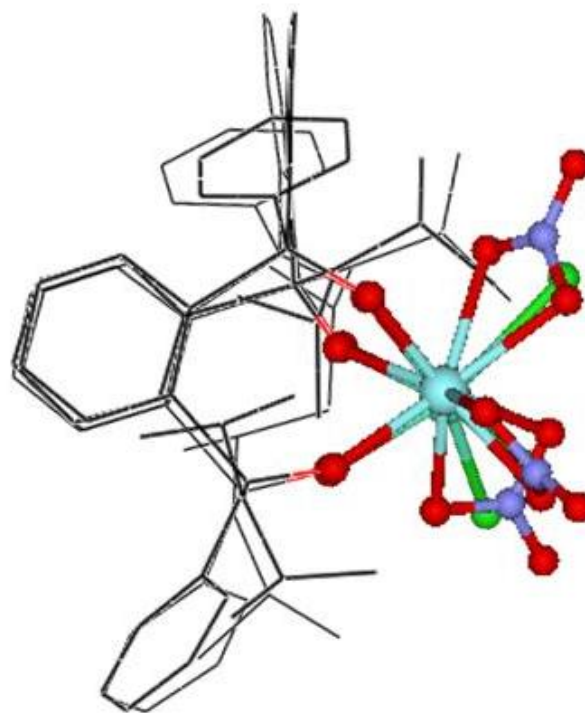


Figure S9. X-ray structures overlay for [Eu(1)Cl₃] (**4**) and [Y(1)(NO₃)₃] (**5**). For complex **5** only one conformation out of the two existing in the asymmetric unit is shown.

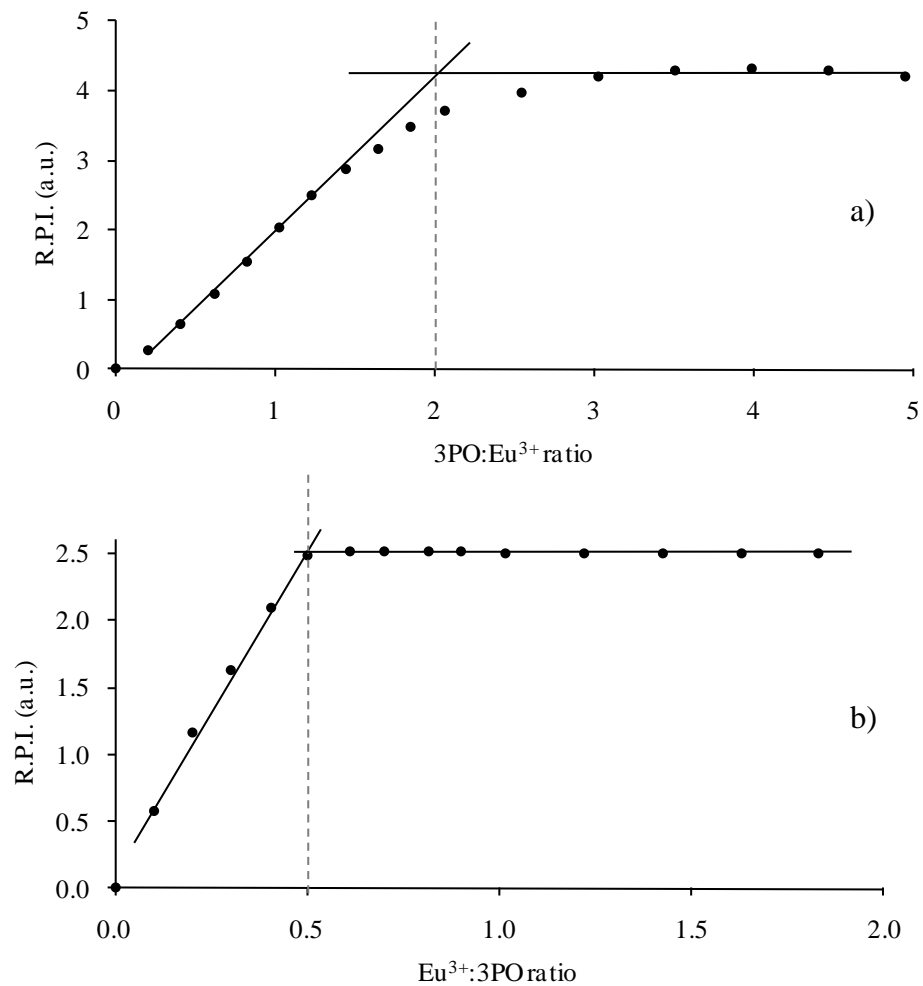


Figure S10. Response of the complex luminescence intensity versus a) Ligand:Eu³⁺ ratio ([Eu³⁺]= 8.0 x 10⁻⁶ M, 75% EtOH, v/v, [NaCl]= 31 mM and pH=7.0); and b) Eu³⁺:Ligand ratio ([Ligand]= 8.3 x 10⁻⁶ M, 75% EtOH, v/v; [NaCl]= 31 mM and pH=7.0).

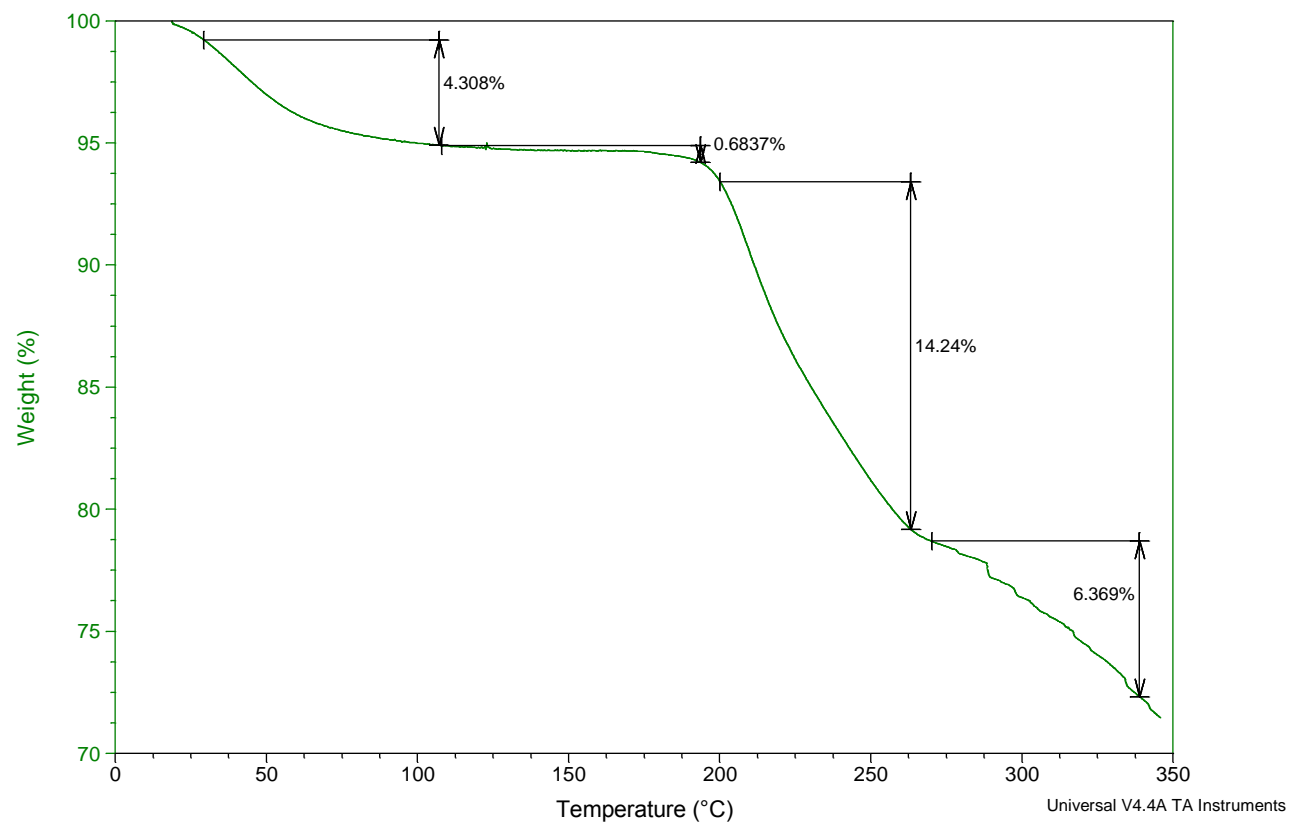


Figure S11. TGA spectrum for complex **2** at the heating rate of 10°C/min under nitrogen atmosphere.

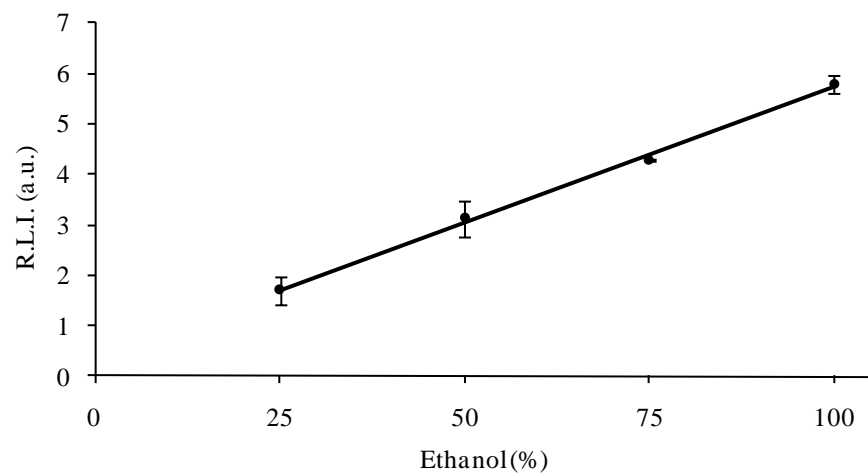


Figure S12. Luminescence intensity versus EtOH percentage in solution. $[\text{Eu}^{3+}] = [\text{Ligand}] = 9.6 \times 10^{-5} \text{ M}$.

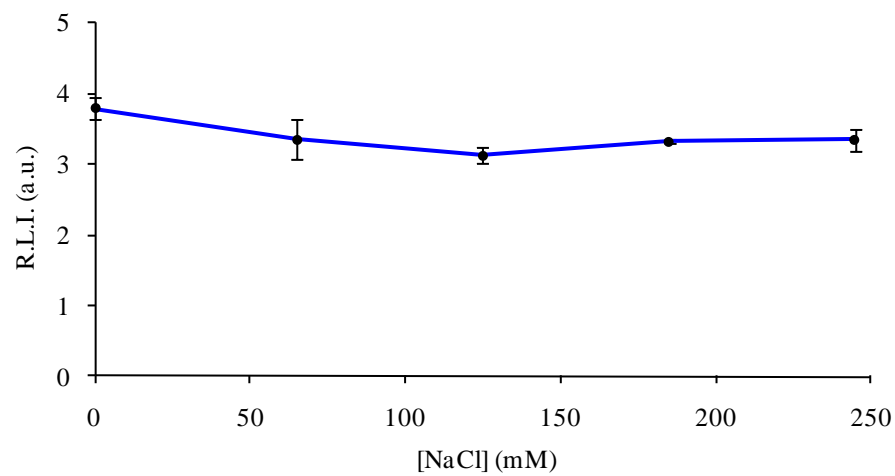


Figure S13. Influence of NaCl concentration on the luminescence intensity in solution. $[\text{Eu}^{3+}] = [\text{Ligand}] = 9.6 \times 10^{-5} \text{ M}$ (75% EtOH, v/v).

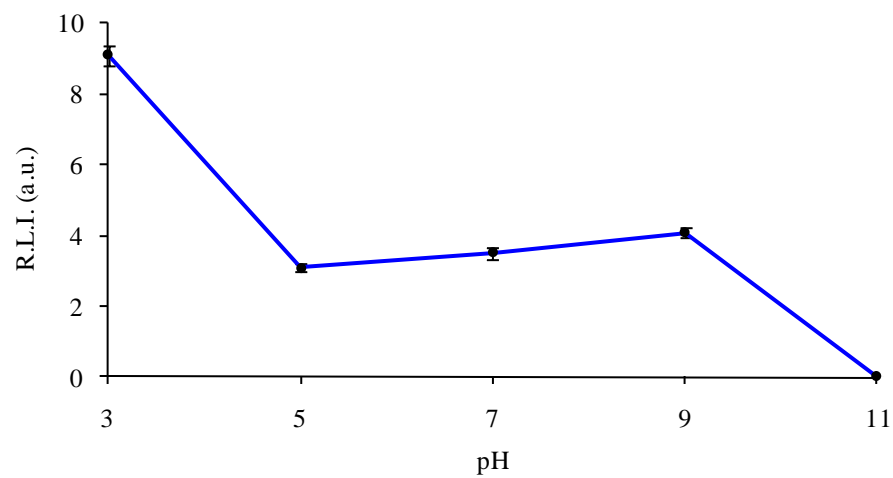


Figure S14. The pH effect on the complex luminescence intensity in solution. $[\text{Eu}^{3+}] = [\text{Ligand}] = 9.6 \times 10^{-5} \text{ M}$ (75% EtOH, v/v; $[\text{NaCl}] = 31 \text{ mM}$).

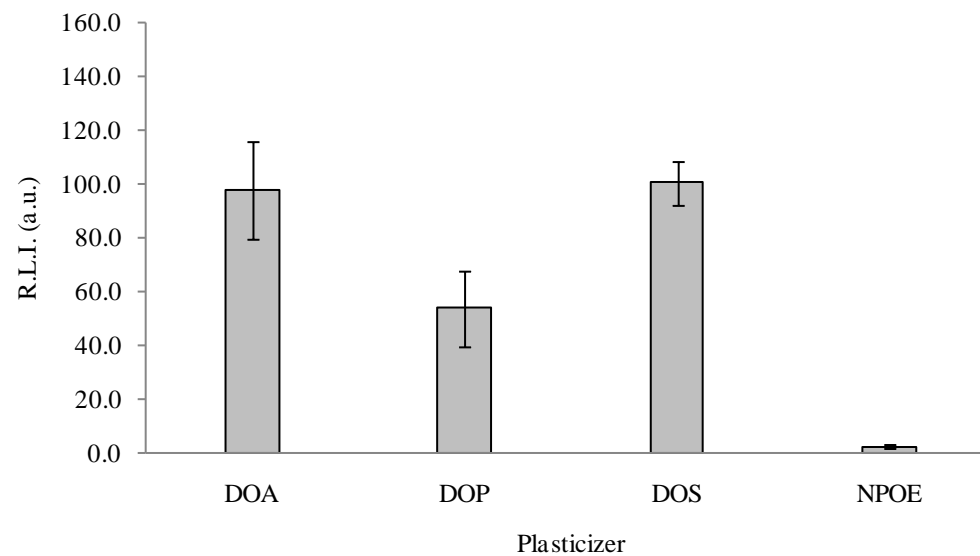


Figure S15. The plasticizer effect on the luminescence signals of the membrane sensors. *DOA* bis(2-ethylhexyl) adipate, *DOP* dioctyl phthalate, *DOS* bis(2-ethylhexyl) sebacate and *NPOE* 2-nitrophenyloctyl ether. Membrane composition: PVC:Plasticizer:Ligand:KTpCIPB as 32.8:64.7:1.5:1.0 (% w/w). $[\text{Eu}^{3+}] = 1.0 \times 10^{-6}$ M in distilled water.

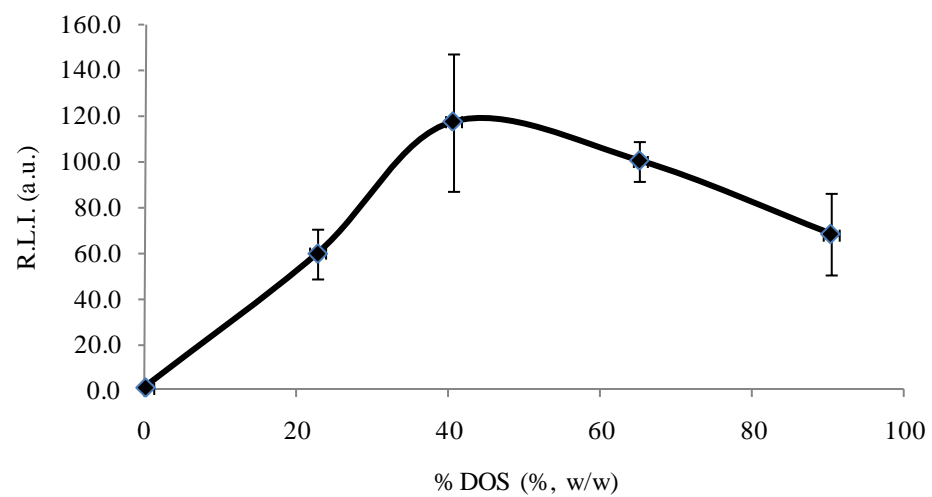


Figure S16. Luminescence intensities of the membrane sensors versus DOS plasticizer percentage. *DOS* bis(2-ethylhexyl) sebacate. Membrane composition: PVC:DOS:Ligand:KTpClPB as 7.5-97.5:0-90.0:1.5:1.0 (% w/w). $[\text{Eu}^{3+}] = 1.0 \times 10^{-6}$ M in distilled water.

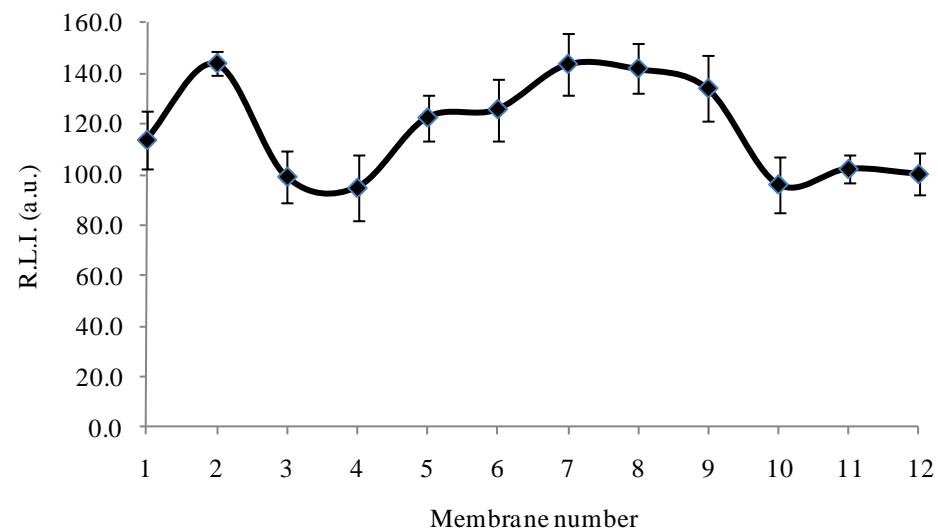


Figure S17. The joint effect of the ligand and ionic additive percentages on the luminescence responses of the membrane sensors. Membrane composition: PVC:DOS:Ligand:KTpCIPB as 27.9-33.4:65.1:1.5-3.5:0-3.5 (% , w/w). $[\text{Eu}^{3+}] = 1.0 \times 10^{-6}$ M in distilled water. Table 2 shows the composition of each membrane.

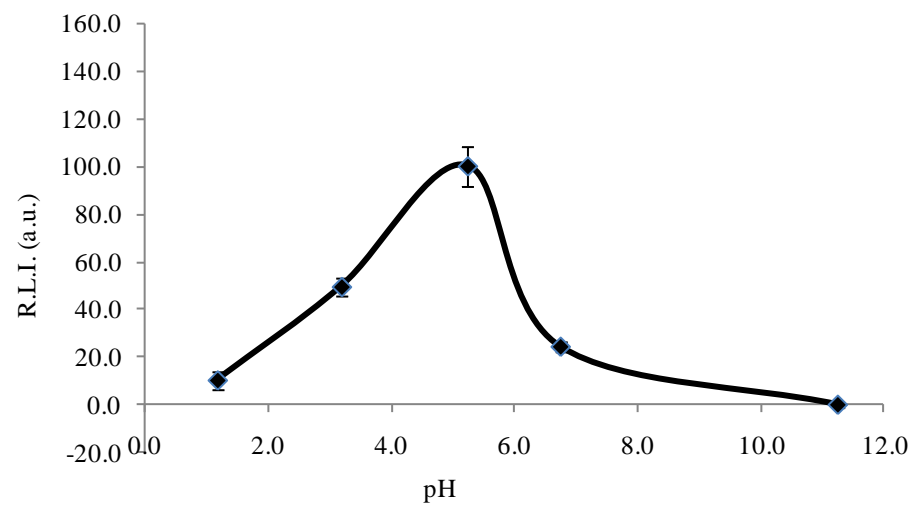


Figure S18. The pH effect on the luminescence signals of the europium sensors. Optimum membrane composition: PVC:DOS:Ligand:KTpCIPB as 33.4:65.1:1.5:0 (% , w/w). $[\text{Eu}^{3+}] = 1.0 \times 10^{-6} \text{ M}$ in distilled water.

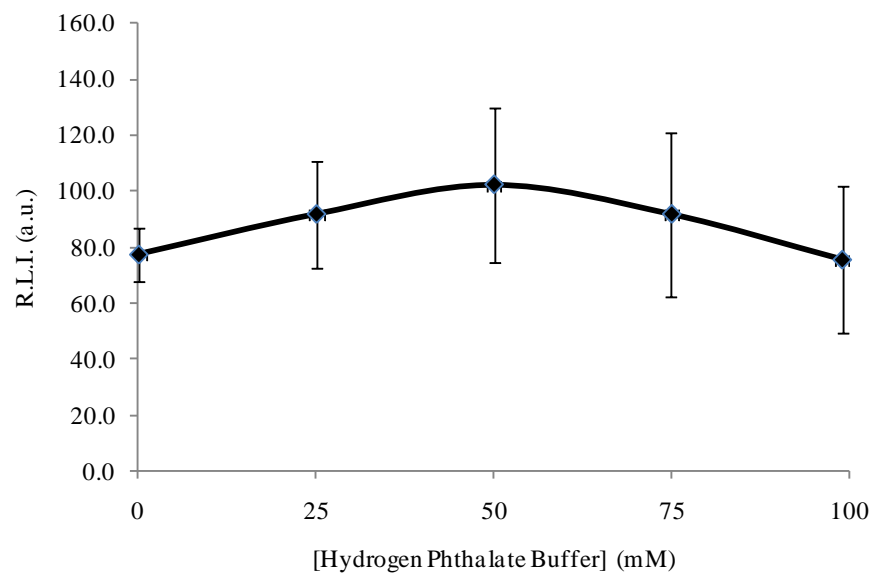


Figure S19. Effect of the ionic strength on the luminescence signals of the membrane sensors. Optimum membrane composition: PVC:DOS:Ligand:KTpCIPB as 33.4:65.1:1.5:0 (% , w/w). $[\text{Eu}^{3+}] = 1.0 \times 10^{-6} \text{ M}$ in distilled water at pH 5.0 and in different hydrogen phthalate buffer concentration solutions at pH 5.0.

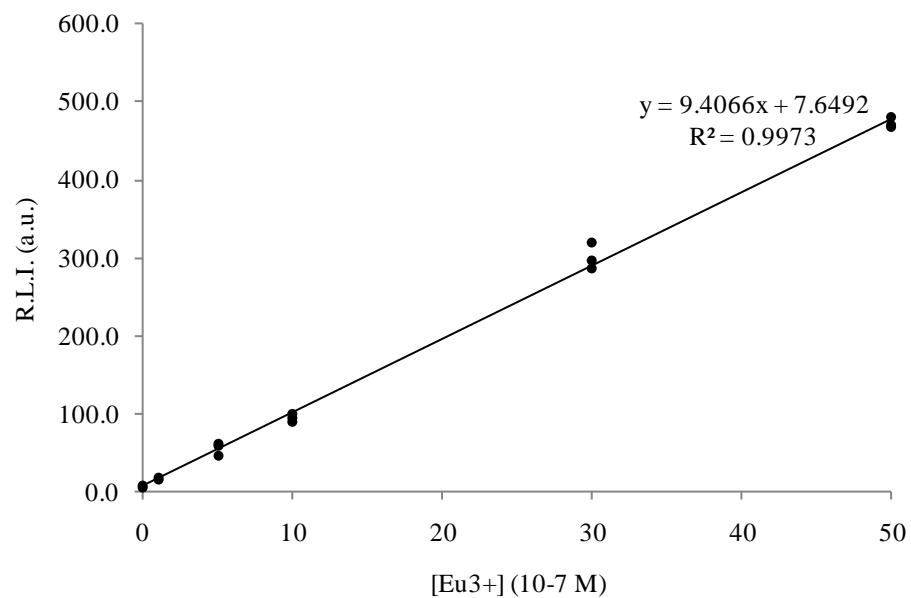


Figure S20. Calibration graph of europium(III) membrane sensors. Optimum membrane composition: PVC:DOS:Ligand:KTpCIPB as 33.4:65.1:1.5:0 (% , w/w). [Blank]= 25 mM hydrogen phthalate buffer at pH 5.0 and $[Eu^{3+}] = 1.0 \times 10^{-7} - 5.0 \times 10^{-6}$ M in 25 mM hydrogen phthalate buffer solution at pH 5.0.

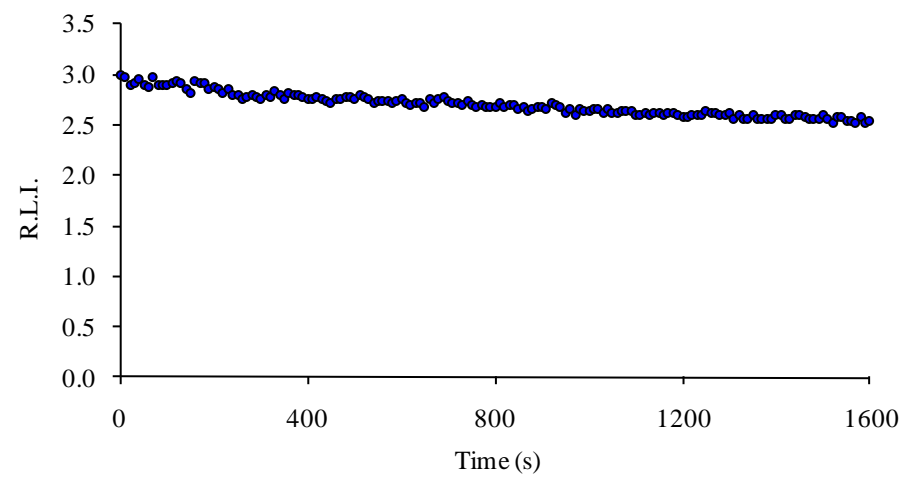


Figure S21. Variation of the luminescence emission in solution versus time.